

Xpikeformer: Hybrid Analog-Digital Hardware Acceleration for Spiking Transformers

Zihang Song, *Member, IEEE*, Prabodh Katti, *Student Member, IEEE*, Osvaldo Simeone, *Fellow, IEEE*,
and Bipin Rajendran, *Senior Member, IEEE*

Abstract—This paper introduces Xpikeformer, a hybrid analog-digital hardware architecture designed to accelerate spiking neural network (SNN)-based transformer models. By combining the energy efficiency and temporal dynamics of SNNs with the powerful sequence modeling capabilities of transformers, Xpikeformer leverages mixed analog-digital computing techniques to enhance performance and energy efficiency. The architecture integrates analog in-memory computing (AIMC) for feedforward and fully connected layers, and a stochastic spiking attention (SSA) engine for efficient attention mechanisms. We detail the design, implementation, and evaluation of Xpikeformer, demonstrating significant improvements in energy consumption and computational efficiency. Through an image classification task and a wireless communication symbol detection task, we show that Xpikeformer can achieve software-comparable inference accuracy. Energy evaluations reveal that Xpikeformer achieves up to a 17.8–19.2× reduction in energy consumption compared to state-of-the-art digital ANN transformers and up to a 5.9–6.8× reduction compared to fully digital SNN transformers. Xpikeformer also achieves a 12.0× speedup compared to the GPU implementation of spiking transformers.

Index Terms—Spiking neural network, transformer, analog-digital hybrid computing, hardware acceleration, energy efficiency.

I. INTRODUCTION

The transformer architecture has revolutionized various fields within artificial intelligence (AI), becoming the cornerstone of many state-of-the-art (SOTA) models used in natural language processing (NLP) [1], computer vision (CV) [2], and wireless communications [3]–[5], but it also imposes a significant burden on computing and memory resources. This is due to their vast number of parameters and the large number of matrix multiplications, particularly during the calculation of the attention mechanism.

The integration of spiking neural networks (SNNs) with transformer architectures represents a promising frontier in the pursuit of energy-efficient and powerful neural computation [6]. SNNs, inspired by the brain’s information processing mechanisms, utilize discrete, temporally-encoded spikes for neuronal signaling [7]. This encoding allows SNNs to achieve higher computational efficiency and lower energy consumption compared to traditional artificial neural networks (ANNs),

which rely on continuous, real-valued activations. *Spiking transformers*, or SNN-based transformers, incorporate spiking dynamics into both feed-forward operations and self-attention mechanisms. They replace traditional multiply-and-accumulate (MAC) operations with accumulate (AC) operations, reducing computational complexity and enhancing efficiency [6], [8]–[16].

Although spiking transformers use simplified computation, they still suffer from inefficiencies when deployed on general-purpose computing platforms like CPUs and GPUs. These inefficiencies arise due to two factors: First, spiking transformers experience significant data communication overhead due to frequent memory access for intermediate results, which worsens with longer spike encoding lengths. Second, spiking transformers utilize binary data, while general-purpose computing platforms operate with higher-precision resources, leading to inefficiency in computation and storage [17]. While optimization efforts for spiking transformers have so far focused on algorithm and software levels, the development of dedicated hardware accelerators remains under-researched.

In recent years, analog in-memory computing (AIMC) using non-volatile memory (NVM) or memristor elements has emerged as a promising mixed-signal approach for accelerating both ANNs and SNNs. AIMC enables matrix-vector multiplications (MVMs) to be performed in constant time, $O(1)$, directly within cross-bar arrays of NVM devices. This is achieved by storing the matrix elements as conductances of the NVM devices and by applying input vector values as electrical voltages to the crossbar input lines and reading the resulting electrical currents in the crossbar output lines, leveraging Kirchoff’s laws [18]. Several AIMC-based ANN transformer accelerators have been proposed, significantly improving the efficiency of ANN transformers [19]–[21]. However, due to architectural differences between ANN transformers and spiking transformers, these accelerators cannot be directly applied to the latter.

Additionally, writing data to memristor crossbars introduces extra latency and energy consumption, and the memristor devices suffer from limited endurance, i.e., they can only support a limited number of read/write cycles before catastrophic failure [22]. Therefore, AIMC is primarily useful for accelerating the inference process in feedforward or fully connected layers, where weights are written to the crossbar once and reused for forward propagation. In the attention mechanism of spiking transformers, the two matrices involved in the matrix multiplication are time-varying activations, making AIMC unsuitable for accelerating this process as the intermediate result storage

The authors are affiliated with the Department of Engineering, King’s College London, London WC2R 2LS, U.K. (zihang.song@kcl.ac.uk, prabodh.katti@kcl.ac.uk, osvaldo.simeone@kcl.ac.uk, bipin.rajendran@kcl.ac.uk)

This work is supported in part by the European Union’s Horizon Europe project CENTRIC (101096379), the EPSRC project (EP/X011852/1) and by Open Fellowships of the EPSRC (EP/W024101/1 and EP/X011356/1).

can quickly exceed the endurance limit [19]. Consequently, designing a new hardware architecture to accelerate the spike-based attention mechanism is necessary.

In this paper, we introduce Xpikformer, a hybrid analog-digital hardware solution specifically designed to accelerate spiking transformers. This architecture combines the strengths of two distinct computing engines to optimize performance and energy efficiency. The AIMC engine handles static-weight operations such as feed-forward, embedding, and fully connected layers, by utilizing specialized memory arrays for efficient data storage and processing. For the attention mechanism, Xpikformer employs the stochastic spiking attention (SSA) engine, which utilizes a simplified computing approach based on logical operations and a streaming dataflow, ensuring fast and efficient processing without the need to store intermediate results.

By integrating these two specialized engines, Xpikformer offers a robust and efficient solution tailored to the unique computational needs of spiking transformers, effectively addressing the inefficiencies found in general-purpose computing platforms. The key contributions of this work are as follows:

- We present Xpikformer, the first hardware architecture for spiking transformers, comprising an AIMC engine and an SSA engine. We also introduce a simulation framework to train and evaluate the accuracy performance of Xpikformer.
- We design spiking neuron tiles within the AIMC engine to efficiently handle feed-forward, embedding, and fully connected layers without storing non-binary pre-activations, thereby significantly reducing data transfer overhead.
- We introduce a software-hardware co-design methodology for spike-based attention architecture, SSA, that builds on stochastic computing and is specifically designed to execute matrix multiplications in the attention mechanism of spiking transformers using lightweight logic gates rather than heavy-weight arithmetic units. We evaluate the proposed SSA tile on an FPGA, demonstrating $18\times$ less latency while consuming $17\times$ less power compared to traditional ANN attention on a GPU.
- We evaluate the energy consumption of the two tasks tested, Xpikformer achieved a $17.8\text{--}19.2\times$ energy reduction compared to the state-of-the-art digital ANN transformer accelerator, a $5.0\text{--}7.1\times$ energy reduction compared to the hybrid implementation of ANN, and a $5.9\text{--}6.8\times$ energy reduction compared to the fully digital implementation of spiking transformers on general-purpose devices. Xpikformer also achieves a $1.53\times$ speedup than traditional ANN on GPU and a $12.0\times$ speedup compared to the GPU implementation of spiking transformers.

This paper is structured as follows: Section II provides an overview of the preliminaries of the work. Section III discusses related work on hardware accelerators for ANN and SNN transformers. Section IV details the design and implementation of the Xpikformer architecture. Section V covers the training and inference methodologies. Section VI presents the accuracy

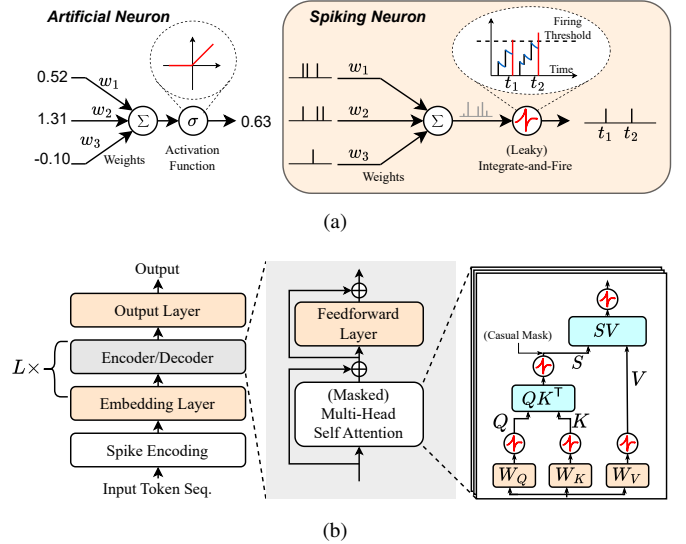


Fig. 1. (a) Illustration of an artificial neuron (left) and a spiking neuron (right). (b) A simplified block diagram of an SNN transformer.

evaluation of the proposed system, and Section VII evaluates its efficiency. Finally, Section VIII concludes the paper.

II. PRELIMINARIES

A. Spike Coding and Spiking Neurons

One essential difference between SNNs and ANNs is the information encoding method. In ANNs, activations are represented by real values x . In contrast, SNNs encode activations in binary temporal sequences $s[t] \in \{0, 1\}$ for $t = 1, 2, \dots, T$, known as *spike trains*, where T denotes the spike encoding length. A commonly utilized spike encoding scheme to map a real value $x \in [0, 1]$ into a spike train is *Bernoulli rate coding*, whereby each bit in the encoded sequence independently takes the value ‘1’ with probability x and ‘0’ with probability $1 - x$, which is expressed as:

$$s[t] \sim \text{Bern}(x) \text{ for } t = 1, 2, \dots, T. \quad (1)$$

Fig. 1(a) illustrates the comparative differences between a spiking neuron and an artificial neuron. Traditional artificial neurons in ANNs aggregate weighted real-valued inputs and apply static activation functions (e.g., sigmoid, tanh, or ReLU) to produce the activation. In contrast, a spiking neuron integrates the weighted sum of input spikes using the leaky integrate-and-fire (LIF) membrane model over discrete time steps. The membrane potential V^t of an LIF neuron at time step t evolves as

$$V^t = \beta V^{t-1} + I^t, \quad (2)$$

where $\beta \in (0, 1]$ represents the leak factor determining the rate of decay of the membrane potential over time, and I^t is the input at time step t . When V^t reaches or exceeds a threshold voltage V_{thresh} , the neuron fires a spike, i.e., $O^t = 1$, resetting the potential V^t to 0. Otherwise, the neuron remains silent, producing $O^t = 0$, i.e.,

$$\text{if } V^t \geq V_{\text{thresh}} \text{ then } \begin{cases} O^t = 1, \\ V^t = 0, \end{cases} \text{ else } O^t = 0 \text{ and (2)}. \quad (3)$$

B. Stochastic Computing

An important advantage of Bernoulli rate coding is that it supports *stochastic computing*, a computational paradigm that employs Bernoulli bit streams [23], [24]. Consider two Bernoulli spike trains $s_1[t]$ and $s_2[t]$ with spiking probabilities $p(s_1[t] = 1) = x_1$ and $p(s_2[t] = 1) = x_2$. The multiplication of real-valued x_1 and x_2 can be achieved by applying the bit-wise logic AND (\wedge) operation on their stochastic representations $s_1[t]$ and $s_2[t]$, which is denoted as:

$$s_{\text{out}}[t] = s_1[t] \wedge s_2[t], \quad (4)$$

since $p(s_{\text{out}}[t] = 1) = p(s_1[t] = 1) \cdot p(s_2[t] = 1) = x_1 x_2$. In this paper, we utilize stochastic computing to help accelerate the matrix multiplications within spiking transformers, as will be detailed in Section IV-B.

C. Transformers and Spiking Transformers

1) *ANN Transformer*: The typical architecture of an ANN transformer model is based on stacks of encoder layers [2], [25], decoder layers [26], or both [1]. Each encoder or decoder layer is composed of a multi-head self-attention (MHSA) mechanism and a feedforward network with residual connections and layer normalization. In models that include both encoder and decoder stacks, the decoder layers also contain an additional multi-head self-attention mechanism that attends to the encoder's output.

The MHSA mechanism in transformers allows the model to compute attention scores that determine the relevance of each token in the input sequence with respect to every other token. This enables the model to weigh and integrate information from different positions in the sequence, capturing various contextual dependencies. Multiple heads attend to the sequence elements on different subspaces simultaneously. For each head, the input token embeddings are projected using projection matrices W_Q , W_K , and W_V to get the query Q , key K , and values V , respectively. The dot-product attention is then calculated as follows:

$$\text{attention}(Q, K, V) = \text{softmax}\left(\frac{QK^T}{\sqrt{d_k}}\right)V,$$

where d_k is the dimension of key vectors within each head.

2) *Spiking Transformers*: Spiking transformers are a novel adaptation of traditional ANN transformers that integrates principles from SNNs [6], [8]–[16]. A typical implementation of a spiking transformer is depicted in Fig. 1(b). In this model, input tokens are initially encoded into temporal spike trains through a spike encoding layer. The subsequent architecture mirrors that of ANN transformers, with the operations of ANN transformers and spiking transformers compared in Table I. The operation of the proposed Xpikeformer is also listed in Table I and will be detailed in Section IV-B.

For a spiking transformer, the feedforward, embedding, and fully connected layers are implemented using spiking neurons in spiking transformers. In the context of MHSA, a notable difference lies in how the token representations Q , K , and V are generated and processed. In ANN transformers, the representations Q , K , and V are obtained through linear projections

applied to the token embeddings X . In contrast, spiking transformers apply LIF neurons after linear projections, resulting in spike-encoded representations Q^t , K^t , and V^t . Compared to the attention score computation $S = \text{softmax}(QK^T/\sqrt{d_k})$ in ANN transformers, spiking transformers first perform matrix multiplication between matrices Q^t and K^t independently for each time step t , and then apply a LIF neuron to the product, which is expressed as $S^t = \text{LIF}(Q^t K^{tT})$. A notable difference in spiking transformer MHSA is the absence of softmax operations. Traditional ANN transformers use the softmax function to normalize the attention scores, ensuring they sum to one. However, in SNNs, the use of softmax is impractical due to the binary nature of spike trains and the need for temporal and sparse processing. Instead, the spiking neurons inherently handle normalization through their spiking activity [10]. The attention score S^t is then multiplied with V^t for every t independently. Then a LIF neuron is applied to obtain the final attention results.

3) *Efficiency Challenges*: Spiking transformers have demonstrated comparable accuracy to their ANN counterparts in fields such as NLP [13], computer vision [12], and wireless communication [27]. These models can provide up to an order of magnitude gain in computational energy efficiency by simplifying the complex floating-point (FP) matrix multiplications of conventional implementations into addition and integer multiplications. However, implementing spike-based models on general-purpose computing platforms, such as CPUs and GPUs, generally leads to significant energy inefficiencies due to the following reasons:

- 1) **Data Communication Overhead**: Spiking transformers do not mitigate the data communication overhead caused by frequent memory access required for storing and reading intermediate results within and between feedforward and MHSA layers. Although intermediate results are mostly one-bit data, this overhead can be exacerbated when the temporal dimension (spike encoding length) exceeds the bit width used in ANNs. Additionally, SNNs generate non-binary pre-activations at every time step, leading to transmission overheads that are T times larger than those in ANNs with the same quantization level, where T is the spike encoding length.
- 2) **Precision Mismatch**: SNNs generate and compute with a large amount of binary data, but general-purpose computing platforms typically use high-precision resources for computation and storage. For instance, CPUs typically operate with 32-bit or 64-bit floating-point (FP32/64) precision. While some GPUs can compute using as low as 8-bit integers (INT8), this is still significantly over-provisioned for handling binary spiking signals. The development of spiking attention accelerators on FPGA devices could potentially address this issue, but this area remains under-researched [28].

D. Analog In-Memory Computing (AIMC)

AIMC enables fast and energy-efficient MVMs using synaptic arrays (SAs). An SA primarily comprises a memristor crossbar. The crossbars consist of memristor devices, which

TABLE I
COMPARISON OF OPERATIONS IN ANN TRANSFORMERS, A TYPICAL SOTA SPIKING TRANSFORMER ARCHITECTURE, AND THE SPIKING TRANSFORMER INTRODUCED IN THIS WORK (GELU = GAUSSIAN ERROR LINEAR UNIT, LIF = LEAKY INTEGRATE-AND-FIRE, BNL = BERNOULLI NEURON LAYER)

Operations	ANN [1]	SNN [8], [10], [12]	SNN (Xpikeformer)
Q, K, V generation	Linear	Linear + LIF	Linear + LIF
Attention	$\text{softmax}\left(\frac{QK^T}{\sqrt{d_k}}\right)V$	$\text{LIF}(\text{LIF}(Q^t K^{t^T})V^t)$	$\text{BNL}(\text{BNL}(Q^t K^{t^T})V^t)$
Feedforward	$W_2(\text{GeLu}(W_1 X))$	$\text{LIF}(W_2 \text{LIF}(W_1 X^t))$	$\text{LIF}(W_2 \text{LIF}(W_1 X^t))$
Inter-layer Normalization	LayerNorm(X)	None	None

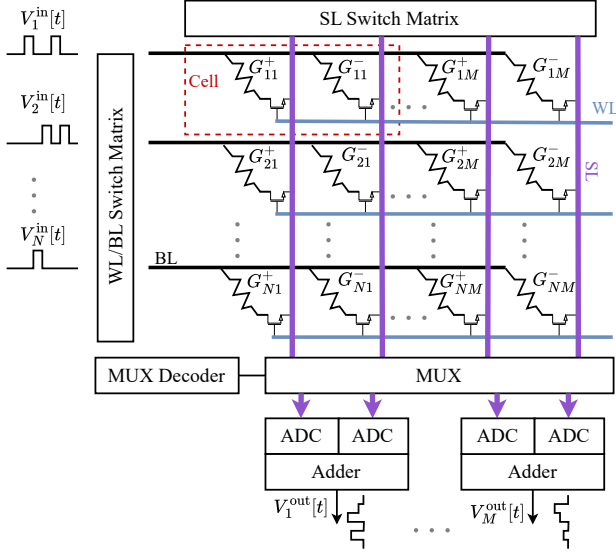


Fig. 2. Illustration of a typical implementation of synaptic array [29] with spike-encoded signals as input.

are NVM elements positioned at the intersections of rows and columns that can be programmed to different conductance levels, representing the matrix elements. This configuration allows the crossbar to store a matrix with significantly greater area efficiency compared to traditional digital buffers. To perform an MVM with a crossbar, the real-valued vector is encoded as input voltages applied to the rows of the crossbar. Ohm's Law governs the current through each memristor, and Kirchhoff's current law (KCL) ensures the correct summation of these currents at the columns, corresponding to the dot-product result. Beyond the crossbar, an SA also includes readout units, which typically comprise successive approximation-register (SAR) analog-to-digital converters (ADCs) coupled with multilevel current-mode sense amplifiers. These are coupled with accumulation circuits, such as adders and registers, as well as various peripheral components, including decoders, multiplexers, switch matrices, and buffers.

A typical implementation of an SA, introduced by [29], is illustrated in Fig. 2. In this setup, every two devices in the crossbar form a differential pair cell, allowing the representation of positive and negative matrix values. The input spike-encoded signals are sent from the bit lines (BLs), and the results are read from the source lines (SLs). The switching on and off of the memristor is controlled by the word line

(WL) and SL through a transistor. During the weighted sum operation, all cells are activated when all WLs are turned on. Input vector voltages are applied to the BLs, and the resulting weighted sum currents are read out through the SLs in parallel. These currents are then digitized by multiple readout units concurrently. To optimize the balance between area, power, and latency, the readout units are shared among a predefined number of crossbar columns and time-multiplexed under the control of a multiplexer (MUX).

In a spiking transformer, input neuron activations are represented by spike trains, which consist of multiple cycles of input voltage signals to the BLs. Because these input signals represent 1-bit binary data at each time step, there is no need to use analog voltages to represent them, thus eliminating the need for digital-to-analog converters (DACs) during inference. However, DACs would need to be provisioned in the hardware to permit the initial programming of the memristor conductances to the required analog levels corresponding to the matrix elements.

III. RELATED WORK

A. ANN Transformer Accelerators

1) *CMOS-based Accelerators*: The development of CMOS-based ANN transformer accelerators primarily aims to enhance computational efficiency. Various strategies have been explored in the literature to achieve this goal. Mixed-precision techniques [30], algorithm-specific quantization [31], and adaptive quantization methods based on input data characteristics [32] have all been utilized. One approach decomposes major operations into a single dot product primitive, allowing for unified and efficient execution, thereby significantly improving throughput [33]. Additionally, an optimized datapath specifically designed for attention mechanisms has been developed, reducing latency and enhancing throughput [32]. Another method addresses inefficiencies in the decoding process by skipping redundant computations and adopting a sparse matrix format to maintain high utilization of MACs [34]. Despite these advancements, the current solutions to the problem of data transfer overhead remain inadequate.

2) *AMIC-Integrated Accelerators*: Advancements in AIMC have significantly enhanced the efficiency and performance of accelerators for ANN transformer models. The most straightforward method leverages AIMC for efficient MVMs in the feedforward layers while retaining the MHSA in general-purpose computing units [35]. This hybrid approach, although

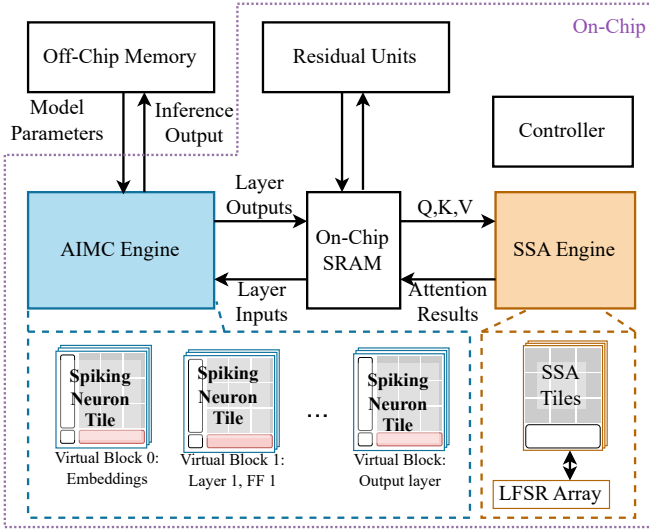


Fig. 3. The overall system architecture of Xpikeformer.

shown to achieve software-equivalent accuracy on NLP tasks, still experiences certain energy inefficiencies due to the high-precision digital computation required for MHSA [36].

Efforts have been made to implement MHSA with AIMC to accelerate the dot-product attention, which necessitates online programming to write the intermediate results K and V into crossbars [19]. Despite a dedicated sub-matrix pipeline designed by the authors, this programming process introduces significant latency and power consumption. Additionally, the wear and degradation of NVM devices render the online-programming approach impractical. A fully circuit-based implementation proposes using functional circuit modules for dot-product attention, softmax, normalization, and activation functions [20], aligning with the feedforward implementations in the crossbar. However, analog circuits introduce significant non-linearity and noise, and require even more power to operate compared to digital complementary metal-oxide-semiconductor (CMOS)-based computations.

Alternative architectures integrate near-memory computing (NMC) or static random-access memory (SRAM)-based digital in-memory computing (DIMC) to manage MHSA workloads [37], [38]. A hybrid in-memory accelerator utilizes eight-transistor (8T)-SRAM to compute MHSA with reduced leakage, employing a sequence-blocking dataflow to enhance hardware utilization and reduce execution time [21]. However, these schemes still require the key (or query) and value matrices to be written to the SRAM array during inference, causing extra latency and energy consumption. Moreover, heavy computing units are still needed to compute the softmax function.

B. Spiking Transformer Accelerators

Despite the extensive research on hardware accelerators for SNNs, particularly for LIF models [39]–[41], the advancement in accelerating spiking transformers remains algorithmic and software-focused. One pioneering study in this domain proposes a spiking MHSA that captures sparse

visual features using spike-form Q , K , and V without employing softmax, achieving accuracy comparable to ANNs in image classification tasks [10], [12]. Another significant contribution [11] presents a hardware-friendly spike-driven residual learning architecture designed to eliminate the non-spike computations introduced by residual connections. Building on these advancements, [16] emphasizes sparse addition operations instead of multiplication in MHSA, further reducing computational energy. However, these aforementioned studies, being at the software and algorithmic level, can be inefficient when deployed on general-purpose computing platforms like CPUs and GPUs due to their intrinsic use of high-precision resources [28]. Moreover, none of these studies have addressed the data transfer overhead, leaving an important aspect of efficiency improvement unexplored. Although FPGA-based spiking attention accelerators offer a potential solution, this area remains underexplored.

IV. XPIKEFORMER ARCHITECTURE

Xpikeformer is a hybrid analog-digital hardware architecture specifically designed for spiking transformers. In the Xpikeformer architecture, two different types of computing engines are employed to handle different operations within spiking transformers, leveraging their respective strengths. The feed-forward, embedding, and fully connected layers are implemented within the AIMC engine, which primarily consists of spiking neuron tiles that include multiple memristor crossbars for storing synaptic weights. The peripheral circuits are optimized to perform accumulation and LIF functionalities without intermediate buffering. The MHSA mechanism is executed by the SSA engine, a framework that leverages stochastic computing to perform dot-product attention operations in the spiking domain. The SSA engine is a purely CMOS-based architecture that uses logical AND gates instead of resource-intensive arithmetic units.

A. AIMC Engine

The AIMC engine is composed of multiple spiking neuron tiles. These tiles are virtually grouped to ensure that each group has sufficient memory to store the weights for one feedforward or fully connected layer. Each spiking neuron tile includes an input and an output buffer, multiple SAs, and a group of LIF units. A shared DAC unit is deployed on each spiking neuron tile to facilitate the initial programming of the SAs, allowing each device to be individually programmed sequentially to achieve multi-bit precision on a single memristor. This DAC unit is bypassed during inference.

1) *Memristor Crossbars*: Each SA within the spiking neuron tile primarily consists of a fixed-sized memristor crossbar, along with multiplexed readout units, as introduced in Section II-D. We impose a restriction on the size of crossbar arrays because excessively large sizes result in increased interconnect resistance and capacitance, higher power consumption, signal degradation, and increased complexity of control circuitry. Consequently, the weights of a feedforward or fully connected layer are most likely distributed across multiple SAs or even several spiking neuron tiles.

TABLE II
CONFIGURATION OF SYNAPTIC ARRAYS

Parameter	Value
Resistive device	PCM
Conductance Resolution	4 bits
Weight Resolution	5 bits
# devices per cell	2
Crossbar dimension (by cell)	128×128
ADC resolution	5 bits
ADC sharing ratio	8

We choose the phase change memory (PCM) device to implement the crossbars in SAs due to its multi-level cell capability (up to 4 bits per device), high endurance, fast read and write speed, and compatibility with CMOS technology [42]–[44]. Detailed SAs configuration parameters of this work are shown in Table II. Nevertheless, as an analog device, PCM suffers from thermal noise, $1/f$ noise, device variability, and quantization effects. A significant challenge associated with PCM is conductance drift, where the conductance of the memory cell changes over time after it has been programmed. This drift can lead to inaccuracies in stored weights and degrade the performance of the neural network, particularly in terms of precision and reliability of the computations. Methods to address the effects caused by these nonidealities will be introduced in Section V.

2) *Weight Mapping and Tile Architecture*: To efficiently manage this distribution and avoid the overhead of storing non-binary pre-activations, we adopt a row-block-wise mapping strategy. For example, with a crossbar size of 128×128 cells and a weight matrix of 384×512 , the weight matrix must be divided into 12 128×128 submatrices. As shown in Fig. 4, the row-block-wise mapping strategy ensures that the same row of submatrices is mapped to the SAs within a single spiking neuron tile. For instance, the 129 to 256 rows of the weight matrix are mapped to four SAs (2-1 to 2-4) within one spiking neuron tile. The input 512×1 vector is then split into four 128×1 subvectors and fed into SA 2-1 to SA 2-4 respectively. At each column output of an SA, only a local sum of the vector dot product can be obtained. To avoid storing this local sum, the outputs of the same column in SA 2-1 to SA 2-4 are routed to the same LIF unit. Thus, all local sums can be directly accumulated within the LIF unit using a carry-save adder (CSA) to get one output feature, i.e. pre-activation. The pre-activation is then added to the current membrane potential via an adder. The new membrane potential overwrites the previous one in a shift register. This value is compared to a threshold stored in the threshold register using a comparator. If the membrane potential exceeds the threshold, the comparator generates a ‘1’ and resets the shift register. For each time step, the shift register is right-shifted by one bit, representing a leak factor of $\beta = 0.5$. The output from the comparator is taken as the output of a spiking neuron, sent to the output buffer, and then sent back to the shared SRAM.

The row-block-wise mapping strategy is compatible with ADC sharing in SAs. In Fig. 4, the sharing ratio is 8, which means each SA has $128/8 = 16$ readout units. Thus, SA 2-1 to SA 2-4 are connected with 16 LIF units. The address

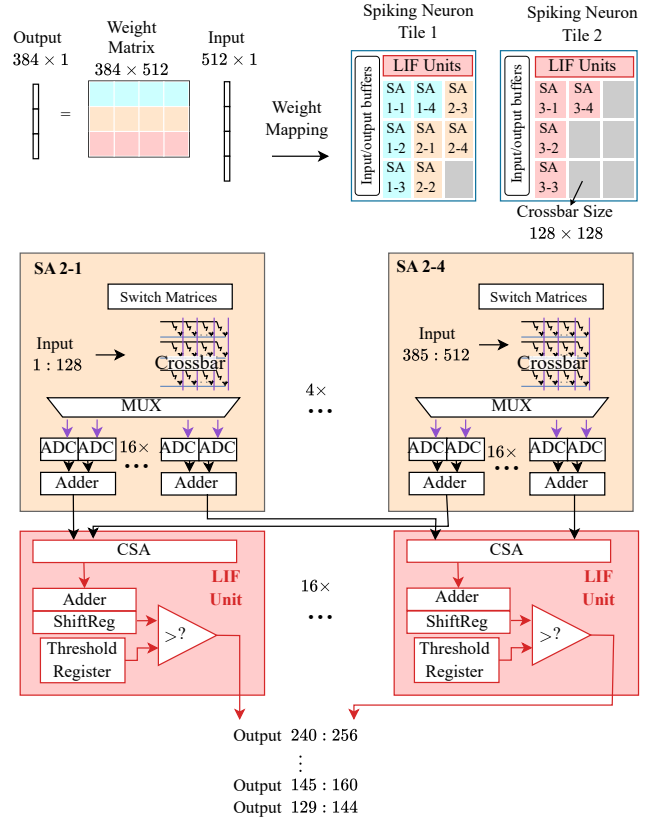


Fig. 4. A illustration of the row-block-wise mapping strategy of synaptic weights.

decoding strategy of the MUX decoder is set as identical over SAs to ensure alignment between local sums. At each MUX decoding cycle, 16 of the 128 output features can be obtained.

By implementing the row-block-wise mapping strategy and utilizing the designed LIF units within the spiking neuron tiles, this design eliminates the significant overhead associated with storing and reading non-binary pre-activations repeatedly, resulting in substantial energy efficiency.

B. SSA Engine

Stochastic spiking attention (SSA) is a software-hardware co-design of the spike-based attention mechanism aimed at minimizing the computing and memory access overhead. SSA is proposed based on the observation that the binary, stochastic nature of the queries Q , keys K , and values V that are projected from Bernoulli-encoded embeddings support efficient multiplication using stochastic computing. We introduce the SSA engine following a bottom-to-top procedure.

1) *SSA Algorithm*: As introduced in Table I, the spiking attention mechanism introduced in [10] evaluate the attention block as:

$$\text{Attention}(Q^t, K^t, V^t) = \text{LIF}(\text{LIF}(Q^t K^{t\top}) V^t), \quad (5)$$

where $\text{LIF}(\cdot)$ represents the per-entry application of LIF neuron as described in Section II-C2. While LIF neurons are stateful, the proposed SSA replaces the LIF neurons with the

Bernoulli neuron layer (BNL), computing the attention results as:

$$\text{SSA}(Q^t, K^t, V^t) = \text{BNL}(\text{BNL}(Q^t K^{t\top}) V^t). \quad (6)$$

A Bernoulli neuron is a stateless neuron that takes real-valued input, normalizes the value to a probability in $[0, 1]$, and then generates a Bernoulli sequence (1) as its output. Using this neuron model, the rate of the output (6) provides an increasingly accurate approximation of real matrix multiplications when Q^t , K^t , and V^t are Bernoulli-encoded and the encoded sequence is sufficiently long.

A detailed description of the SSA algorithm is shown in Algorithm 1. Owing to the binary nature of the representations Q^t , K^t , and V^t , the matrix multiplications in (6) are realized by lightweight logic AND operations and additions instead of real multiplications. In step 5, the $N \times N$ binary attention scores S^t are obtained by first calculating the dot-product between Q^t and K^t . This is done by summing the results of logical AND operations across the dimension d_K . The result is then normalized and used for Bernoulli encoding. Step 9 applies a similar logical AND to compute the matrix multiplication between S^t and V^t and generate probabilistically encoded attention result A^t .

Algorithm 1 Stochastic Spiking Attention (SSA)

- 1: **Input:** $d_K \times N$ binary matrix sequences Q^t, K^t, V^t for $t = 1, \dots, T$, dimension d_K (corresponding to one attention head)
 - 2: **Output:** $d_K \times N$ binary matrix sequence A^t for $t = 1, \dots, T$ (corresponding to one attention head)
 - 3: **for** $t = 1$ to T **do**
 - 4: **for** each (n, n') in $N \times N$ **do**
 - 5: $S_{n, n'}^t \sim \text{Bern}\left(\frac{1}{d_K} \sum_{d=1}^{d_K} Q_{d, n}^t \wedge K_{d, n'}^t\right)$
 - 6: **end for**
 - 7: Apply casual mask if using a decoder
 - 8: **for** each (d, n) in $d_K \times N$ **do**
 - 9: $A_{d, n}^t \sim \text{Bern}\left(\frac{1}{N} \sum_{n'=1}^N A_{n, n'}^t \wedge V_{d, n'}^t\right)$
 - 10: **end for**
 - 11: **end for**
-

2) *SSA Tile*: We designed a customized hardware architecture, referred to as SSA tiles, optimized for SSA operations. As illustrated in Fig. 5, SSA tiles streamline the computation of spike-based attention by utilizing bitwise logic devices. This design effectively eliminates the data transfer overhead caused by writing and reading intermediate results, significantly enhancing both the energy efficiency and performance of the computations.

Each SSA tile is composed of N^2 physical stochastic attention cells (SACs) arranged as an $N \times N$ array. The N^2 parallelization level in SACs offers significant benefits. First, it enables simultaneously sending each query to each key-value pair. This is achieved by simultaneously streaming K^t and V^t across columns and Q^t across rows via 1-bit data buses. Furthermore, it allows for the parallel computation of all $N \times N$ elements of the attention score S^t matrix. The (i, j) -th element of matrix S^t is computed within the corresponding (i, j) -th SAC. This efficient data streaming through the SSA

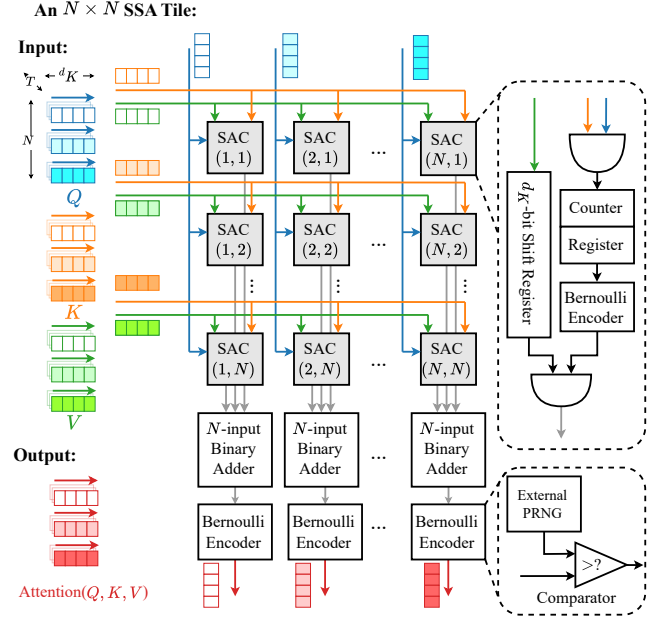


Fig. 5. Block diagram of an $N \times N$ SSA tile.

block eliminates the need for writing/reading intermediate data from the memory. Since SOTA transformers for edge AI applications have N in the range of $16 - 128$, we have employed N^2 physical SAU units in our design.

To calculate the (i, j) -th element of S^t , totally d_K AND operations are needed between the elements of the i -th row of Q^t and the j -th row of K^t . These d_K AND operations are executed serially in time within the (i, j) -th SAC via an AND gate. The summation is realized by counting the AND output using a counter with unsigned INT8 (UINT8) output, accommodating a key dimension d_K up to $2^8 = 256$. After every d_K clock cycles, the summation is buffered to a Bernoulli encoder, where it is normalized by d_K and used as a probability to generate the Bernoulli sample $S_{i, j}^t$.

To calculate the attention output A^t , the generated attention scores $S_{i, j}^t$ are held in the SAC for d_K clock cycles. The local attention result between $S_{i, j}^t$ and the j -th row of V^t is calculated using another AND gate, serving as the output of the SAC. To avoid using external delays for V^t , a d_K -bit shift register operating on a first-in-first-out basis is deployed in each SAC to temporarily buffer V^t and align it with S^t . This allows for the simultaneous streaming of Q^t , K^t , and V^t within the SSA block, facilitating pipelining over time steps. The summation of the local attention results is achieved by adding the outputs of each column of SACs using an N -input binary adder. The sum is then sent to another Bernoulli encoder, where it is normalized by N and used as a probability to generate the Bernoulli samples. The i -th row of A^t is generated sequentially by holding $S_{i, j}^t$ in the (i, j) -th SAU when streaming the j -th row of V^t . As a result of this procedure, the i -th column within the SSA tile sequentially outputs the i -th row of the attention result A^t . With N rows of SACs operating in parallel, the entire matrix A^t is calculated column by column by one SSA tile.

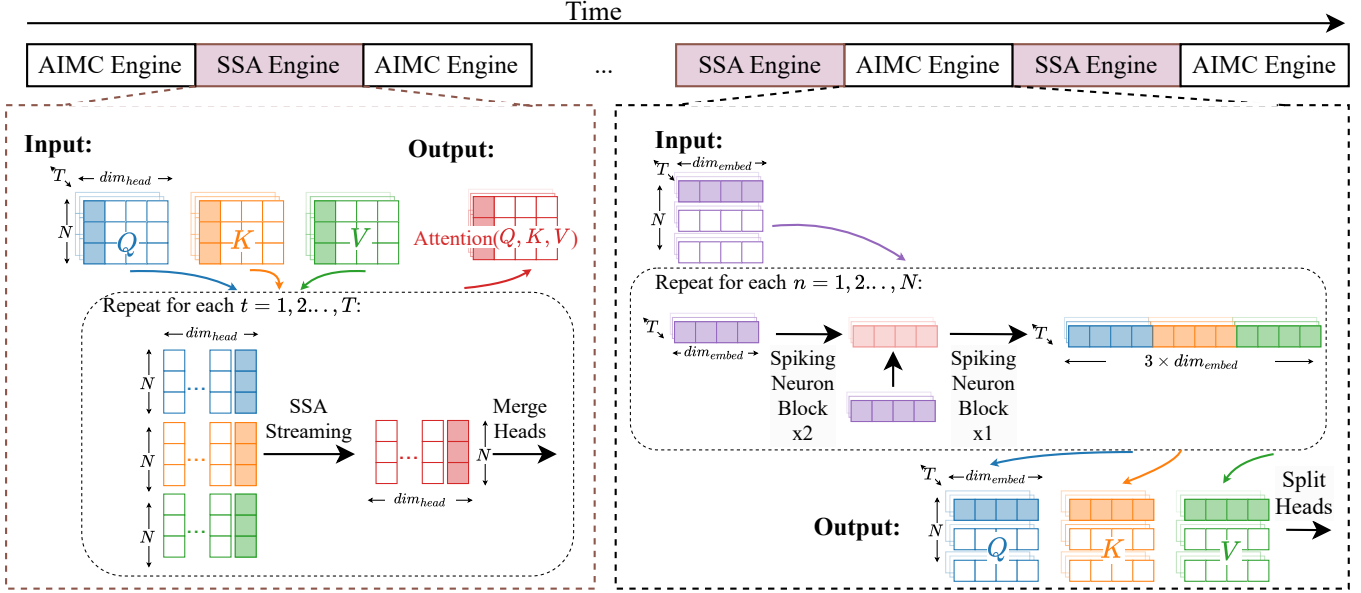


Fig. 6. Illustration of Xpikeformer inference dataflow.

The Bernoulli encoder in our design uses a comparator to compare the input integer with a pseudo-random number (PRN) generated from an external source. Notably, we do not perform normalization in hardware; instead, we directly compare the unnormalized input integer I with a random integer sampled uniformly from $(0, I_{\max}]$. In our design, I_{\max} is set to d_K within SACs and to N outside of SACs. Choosing d_K and N as powers of two can streamline the hardware design by allowing us to directly use a fixed-point random integer sampled from a uniform distribution for the comparison. This approach simplifies the design and enables the use of power-efficient Linear Feedback Shift Register (LFSR)-based PRN generators.

3) *SSA Engine*: The SSA engine is designed for efficient execution of self-attention mechanisms in transformer models. It consists of multiple SSA tiles, each serving as an individual attention head. These tiles are stateless, allowing them to be reused across different layers of the Transformer, which significantly enhances both area and energy efficiency. Additionally, the SSA engine incorporates an LFSR array that generates all the necessary PRNs for the Bernoulli neurons, ensuring a consistent supply of random numbers required for the stochastic elements of the model.

To further optimize power and area efficiency, the SSA engine implements a custom reuse strategy for random number generation, as described in [45]. Here we implement a 32-bit LFSR and tap all 4 bytes from the LFSR instead of just the lowest 8-bits [46]. This approach maximizes the utilization of generated random numbers, conserving both power and silicon area. By leveraging these design strategies, the SSA engine achieves a balance of high performance and resource efficiency.

C. Dataflow

Fig. 6 illustrates the inference data flow of Xpikeformer, featuring the alternating operation of the AIMC engine and the SSA engine, with data exchange facilitated through on-chip SRAM.

The AIMC engine serially drives input data through each forward propagation or fully connected layer. Each AIMC cycle, except for the first and last, includes two feedforward layers and one fully connected layer to project embeddings into the QKV feature space. In each layer, data is input in a “token-wise event-driven” manner: the spike encoding of the same token embedding is input sequentially over T time steps, followed by cycling through N tokens. This approach allows the membrane potential stored in the LIF unit’s register to accumulate directly and reset upon token switching. Looping N tokens for each time step t would require storing and reading back membrane potentials, leading to unnecessary data transmission overhead.

Between layers within the same AIMC engine, N token embeddings are forwarded in a pipelined manner. During the forward transmission of each token embedding, the spike encoding over T time steps is also pipelined between layers.

The SSA engine operates multiple SSA tiles in parallel, with each tile handling one head of the multi-head attention mechanism. As previously discussed, Q , K , and V data in SSA tiles are transmitted in a “matrix-wise event-driven” manner. The three matrices Q^t , K^t , and V^t are streamed to the SSA tile column by column over d_K clock cycles. The subsequent matrices Q^{t+1} , K^{t+1} , and V^{t+1} are transmitted in the next d_K clock cycles. When pipelining in time steps, the computational delay of an SSA tile (from first input to first output) is approximately d_K , ensuring high computational efficiency of the SSA engine.

V. TRAINING AND INFERENCE DETAILS

A. Integrated Framework for Hybrid Training

To effectively train Xpikeformer, we adopt a hybrid framework that integrates *SpikingJelly* [47] and the *IBM Analog Hardware Acceleration Toolkit* (AIHWKit) [48]. SpikingJelly defines and manages the spiking components of Xpikeformer, particularly the LIF neurons and the SSA. AIHWKit is adopted to simulate the nonidealities inherent in AIMC.

We adopt a two-stage training procedure – at the initial training stage, conventional training (CT) is used in an ideal full-precision digital environment using SpikingJelly. After obtaining the trained parameters, AIHWKit is used to conduct hardware-aware training (HWAT) to fine-tune the parameters. This is achieved by injecting noise in the forward propagation while keeping the backward propagation ideal. This procedure adapts the network parameters to realistic PCM-based hardware imperfections.

During training, the forward propagation outputs are averaged over time steps to calculate the loss, with the loss function defined similarly to that in training ANN transformers. The Adam optimizer is employed to train the Xpikeformer network [49].

B. Global Drift Compensation

To address the conductance drift of the PCM devices over time in the AIMC engine, we implement a global drift compensation (GDC) method introduced in [50]. During the calibration phase, we periodically measure the total current of several columns in each SA programmed to known conductance values. This allows Xpikeformer to track global shifts in conductance. During inference, the outputs are scaled by a factor derived from these calibration measurements. The calibration can be performed while the PCM array is idle, with the summation of currents implemented within the control unit of the system.

VI. ACCURACY EVALUATION

A. Tasks Description

The inference accuracy of Xpikeformer is validated in hardware-simulated environments using AIHWKit. We assess the encoder-only and decoder-only architectures separately through two respective tasks.

Task 1 (Image Classification): To evaluate the accuracy performance of the encoder-only Transformer, we select an image classification task as it requires the model’s ability to extract and process relevant features from the entire input image in parallel. We utilized an SNN-based vision transformer (ViT). We selected the CIFAR-10 dataset, which comprises 10 different classes of objects.

Task 2 (In-context Learning for Wireless Communication): Decoder-only transformers are often used for tasks involving temporal sequential dependencies. A notable ability of these models is in-context learning (ICL). As illustrated in Fig. 7, the model is provided with a sequence of query-answer pairs that follow a consistent pattern, even though the model has not been explicitly trained on this pattern. The model is

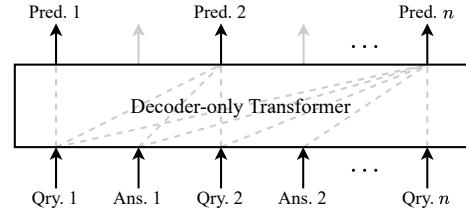


Fig. 7. A conceptual illustration of in-context learning (ICL) using a decoder-only transformer.

TABLE III
MODEL CONFIGURATION PARAMETERS FOR TASK 1 AND TASK 2

Parameter	Task 1	Task 2
Token dimension	48	4
Embedding dimension	512	256
Hidden dimension	2048	1024
# layers	6	4
# heads	8	8
# classes	10	16
Attention mask	Casual mask	Diagonal mask

then expected to predict the answer for a new query by attending to the preceding query-answer pairs within the input sequence. This ability has been demonstrated to enable wireless receivers to correctly classify symbols after they have undergone unknown wireless channels and been contaminated by nonlinearities [3], [4]. We adopt the symbol detection task as formulated in [27] and evaluate accuracy performance using the bit error rate (BER) metric (a lower BER indicates higher accuracy). We fix the number of input query-answer pairs to 18. An SNN-based GPT-2-like decoder-only transformer is employed, with size parameters detailed in Table III.

B. Accuracy Results

Due to the noise, variability, and non-linearities of analog computations, the inference accuracy of Xpikeformer is inherently lower than that of full-precision digital computations. For Task 1, we train the SNN-based ViT on the CIFAR-10 training set from scratch, using the HWAT strategy as introduced in Section V-A. We test the inference accuracy on the evaluation dataset using the simulation platform as described in Section V-B. For Task 2, the decoder-only model is trained on a training dataset that is generated from a set of 8192 wireless channels and tested on a dataset generated from another 1024 wireless channel distinct from the training dataset. We compare the Xpikeformer results with two baseline implementations: (i) ANN (Digital) – A traditional ANN transformer trained and tested on fully digital devices; (ii) SNN (Digital) – an SNN transformer trained and tested on fully digital devices, with its attention implemented by SSA. The parameters of both baselines are INT8-quantized.

For Task 1, we evaluated image classification accuracy over different spike encoding lengths, T . Fig. 8(a) presents the accuracy of SNN (Digital) and Xpikeformer across varying spike encoding lengths, compared to the baseline digital ANN, which achieved an accuracy of 86.02%. Both Xpikeformer and its fully digital counterpart demonstrate increasing accuracy with longer encoding lengths. Xpikeformer shows converging

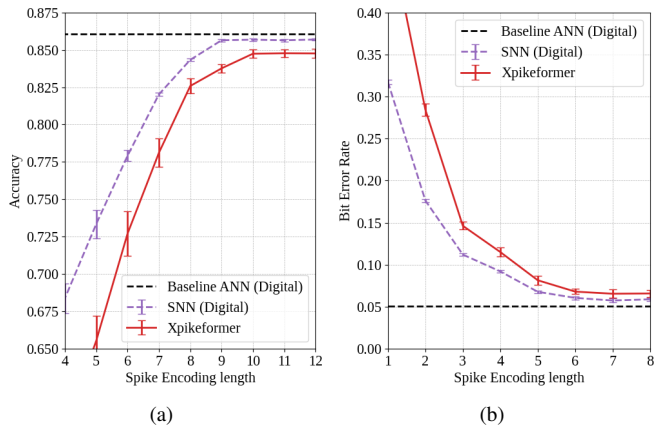


Fig. 8. (a) CIFAR-10 classification accuracy in Task 1 and (b) bit error rate in Task 2 versus spike encoding length for SNN (Digital) and Xpikeformer. Baseline ANN results are shown for comparison.

accuracy (84.74%) at $T = 10$, which is only 1% lower than the 85.68% accuracy achieved by SNN (Digital) at the same spike encoding length. The error bars indicate standard deviations from multiple tests, decreasing with longer encoding lengths for both SNN models. The uncertainty in the SNN (Digital) results arises from the Bernoulli encoder used in SSA. Xpikeformer exhibits higher uncertainty in accuracy performance compared to SNN (Digital) due to additional AIMC hardware noise, but this uncertainty reduces to less than 0.003% at $T \geq 10$, sufficiently small for stable inference.

Similarly, in Task 2, we observe that Xpikeformer shows converging BER when the spike encoding lengths $T \geq 6$, as shown in Fig. 8(b). Compared to the 0.051 BER achieved by the baseline ANN (Digital), SNN (Digital) and Xpikeformer achieve BERs of 0.061 and 0.067, respectively, at $T = 6$, which are sufficiently low for the task. Increasing the spike coding length T further improves accuracy slightly, with a tradeoff in latency and energy. This tradeoff should be considered in practical designs.

C. Long-term Accuracy Performance

We evaluated the accuracy of memristor devices over time to investigate the impact of different training strategies and drift compensation methods. The experiment involved testing four spiking transformers, all based on the Xpikeformer architecture. These transformers were trained using two distinct strategies (CT and HWAT) and evaluated during inference with and without the application of the GDC compensation method. The results for Task 1 are shown in Fig. 9(a). Without GDC and HWAT, the accuracy started at 79.70% right after programming and showed a significant drop to below 70% within an hour. With HWAT but no GDC, the accuracy remained above 84% for at least one minute but decreased to below 80% within one hour due to conductance drift. With GDC but no HWAT, the model achieved up to 84.30% accuracy and maintained it above 70% within a year. With both GDC and HWAT, the accuracy was preserved at 81.13% after one year, dropping by only 3.6%. Similar results for Task 2 are shown in Fig. 9(b), demonstrating that the BER

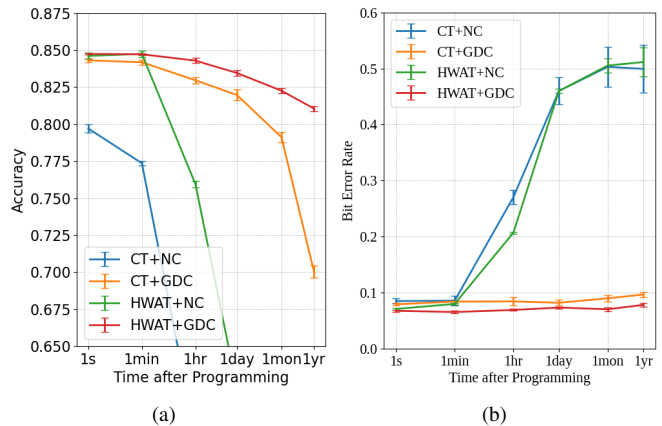


Fig. 9. Accuracy performance of the hybrid implementation of SNN transformer trained with different strategies and drift compensation methods: conventional training (CT) + no compensation (NC), CT + global drift compensation (GDC), hardware-aware training (HWAT) + NC, and HWAT+GDC for (a) Task 1 and (b) Task 2.

can be maintained at a low level, less than 0.08, for at least one year after writing weights to the devices when HWAT and GDC are applied. These findings suggest that with HWAT and GDC, Xpikeformer does not require frequent reprogramming to maintain high performance, thereby reducing maintenance costs and increasing the overall reliability of the hardware.

VII. EFFICIENCY EVALUATION

A. Energy Consumption

We evaluate the runtime energy consumption of the entire network in two parts: *computational energy* and *runtime memory access energy* consumption.

1) *Baselines*: We compare the runtime energy consumption of Xpikeformer with four baseline architectures: (i) ANN-Digital – a SOTA fully digital ANN transformer accelerator as reported in [31]; (ii) ANN-Hybrid – replacing the feed-forward and fully connected layers in (i) with AIMC crossbars. (iii) SNN-Digital (no SSA) – a fully digital implementation of SNN transformer with dot-product attention implemented with integer adders. (iv) SNN-Digital (with SSA) – a fully digital implementation of SNN transformer with dot-product attention implemented with SSA.

2) *Evaluation Methods*: For the AIMC crossbars used in both Xpikeformer and the baseline configuration (ii), we customize the *DNN+NeuroSim V1.4* framework [29] with the parameters specified in Table II to simulate the hardware implementations on a layer-by-layer basis. The area and energy estimates of the SSA tile were obtained by performing synthesis using the Cadence 45nm process design kit (PDK).

To estimate the baseline energy consumptions, we consider all digital operations (MAC, AC, MUL, ADD, and logic gates) using energy metrics based on 45 nm CMOS technology as reported in [51], [52], following the approach in [53]. We assume that there is sufficient on-chip cache to keep the model weights loaded for the entire duration of the hardware operation. Therefore, the energy consumption for loading model parameters is excluded from our runtime

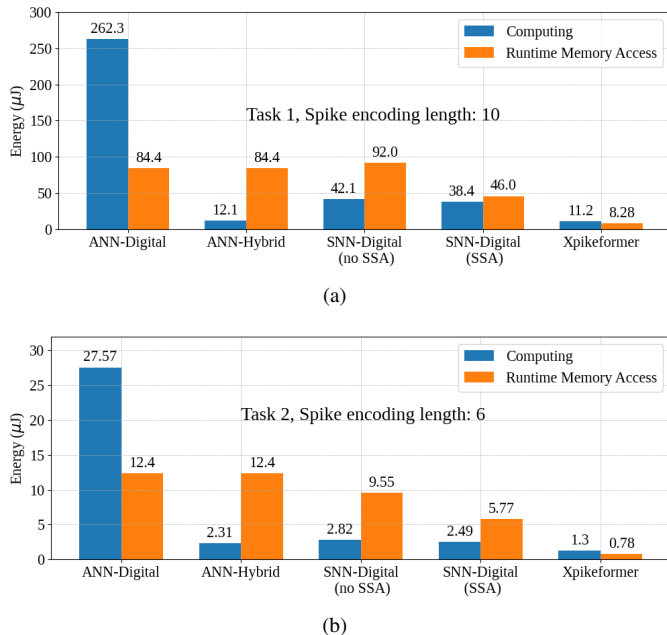


Fig. 10. Energy consumption comparison between Xpikformer and baseline implementations.

memory access energy calculations. For all memory access operations required to read or write input data, output data, and intermediate results, we assume that all necessary data is read from or written to the on-chip SRAM. For all input data, output data, and intermediate results in ANNs, as well as pre-activations in SNNs, we assume they are quantized to INT8 and stored in 8-bit SRAM when necessary. For the fully digital configurations (i), (iii), and (iv), we assume all model parameters are also quantized to INT8 and pre-loaded into the cache.

3) *Results*: We evaluate the energy consumption on both Task 1 and Task 2. One main difference between Task 1 and Task 2 is the architectural parameters of the transformer networks, as detailed in Table I. For Task 1, a ViT-small encoder-only network is used, featuring 512 embedding dimensions, 6 layers, and 8 attention heads in each MHSA block. Task 2 employs a much smaller decoder-only network, differing from Task 1 by having 2 fewer layers, and a 2× lower embedding dimension while maintaining the same number of attention heads. Additionally, Task 2 employs a shorter spike encoding length during inference, $T = 6$, compared to $T = 10$ in Task 1, as this was determined to be the minimum length required to achieve the desired accuracy, as discussed in Section VI.

The energy consumption comparisons between Xpikformer and the baseline implementations for Task 1 and Task 2 are shown in Fig.10(a) and Fig.10(b), respectively. Several key insights can be drawn from comparing the baseline implementations. Firstly, the spike encoding length plays a crucial role in converting ANN to SNN in the digital domain, with both computing energy and runtime memory access energy of a digital spiking transformer being directly proportional to it. In an ANN-Digital configuration, MAC operations account for over 99% of the total computing energy. By replacing these energy-intensive MAC operations with more efficient AC

operations, the SNN-Digital (no SSA) achieves significantly lower computing energy – about $6.3\times$ lower in Task 1 and $10.1\times$ lower in Task 2. This reduction is approximately inversely proportional to the spike encoding length used in the tasks.

From a data communication perspective, while the softmax-free design of spiking transformers reduces some storage overhead for intermediate results, SNN-Digital (no SSA) incurs even higher runtime memory access energy ($1.1\times$ that of ANN-Digital) in Task 1. This is because the spike encoding length ($T = 10$) adopted in Task 1 requires SNN-Digital (no SSA) to transfer binary data 10 times between layers, whereas the digital ANN only needs to transfer INT8 data once, making it less demanding in terms of memory access. Additionally, the burden of moving non-binary pre-activations 10 times significantly impacts SNN-Digital (no SSA), constituting approximately 40% of the total runtime memory access energy. Conversely, in Task 2, SNN-Digital (no SSA) consumes less runtime memory access energy ($0.8\times$ that of ANN-Digital) because intermediate results and pre-activations only need to be stored and retrieved $T = 6$ times, compared to the $T = 10$ cycles required in Task 1.

Considering the energy efficiency for computing, note that in Task 1, the attention operation in SNN-Digital (no SSA) consumes approximately $5 \mu\text{J}$ out of the total $43.1 \mu\text{J}$ computing energy. With the implementation of SSA, this $5 \mu\text{J}$ is significantly reduced to around $1 \mu\text{J}$, resulting in a total computing energy of $38.4 \mu\text{J}$. Similarly, in Task 2, attention contributes about $0.5 \mu\text{J}$ to the total computing energy in SNN-Digital (no SSA), which is reduced by $0.33 \mu\text{J}$ with SSA. Overall, SSA achieves a 3–5× reduction in energy consumption compared to spiking attention using AC operations.

The energy efficiency of SSA also stands out in terms of runtime memory access energy owing to the streamlined design of SSA tiles, which eliminates the need to store attention score S^t and its pre-activations. This reduces the overall runtime memory access by $2\times$ in Task 1 and $3.4\times$ in Task 2.

To further improve the overall energy budget, the proposed Xpikformer architecture incorporates an AIMC engine in addition to being equipped with SSA. This further reduces the overhead of intensive CMOS AC operations through AIMC, achieving the lowest computing energy consumption in both tasks. For runtime memory access energy, the streamlined integration between SAs and LIF units in Xpikformer minimizes the need to write and read non-binary pre-activations over T cycles, resulting in significantly reduced runtime memory access energy. Compared to SNN-Digital (SSA), Xpikformer archives approximately $5.6\times$ and $7.4\times$ reduction in runtime memory access energy in Task 1 and Task 2, respectively.

Xpikformer outperforms the other AIMC-integrated architecture, ANN-Hybrid, in energy efficiency primarily by eliminating the need for intermediate results storage. While ANN-Hybrid utilizes AIMC for feedforward operations and Q , K , and V mapping, it still requires the storage of attention intermediate results (QK^T , scaling results, softmax intermediate results, attention scores) and the output of the first layer in the feedforward blocks. These storage requirements are identical

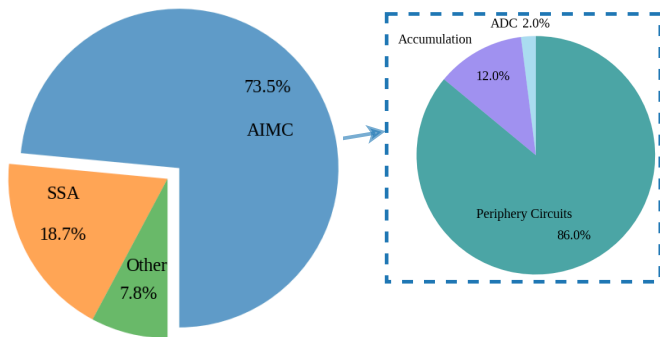


Fig. 11. Breakdown of Xpikeformer computational energy.

to those of ANN-Digital. In contrast, Xpikeformer eliminates the storage overhead of attention intermediate results by computing in the spike domain, aided by streamlined SSA tiles, and removes the need to store pre-activations in feedforward blocks through the integration of SAs and LIF units within the AIMC engine.

It is worth noting that ANN-Hybrid exhibits competitive computing energy consumption. In Task 1, the computing energy of ANN-Hybrid ($12.1 \mu\text{J}$), which uses INT8 activations, is comparable to that of Xpikeformer ($11.2 \mu\text{J}$), which employs $T = 10$. The slight overhead in ANN-Hybrid is due to the complexity of GeLu, normalization, and softmax operations. However, this advantage diminishes when the corresponding spiking transformer requires a shorter spike encoding length (compared to the ANN data quantization bitwidth) to achieve satisfactory accuracy. For example, in Task 2, Xpikeformer only needs $T = 6$, while ANN-Hybrid requires 8 AIMC cycles to process INT8 feedforward operations. Additionally, the complex digital activation functions and normalization in ANN-Hybrid reduce its competitiveness in computing energy for this task.

Fig. 11 presents the breakdown of Xpikeformer computational energy consumption. The majority of the computing energy is consumed by the AIMC engine, accounting for 73.5% of the total computational energy. The SSA engine contributes 18.7%, while other components, such as residual units, collectively account for 7.8%. A more detailed breakdown of the AIMC engine’s energy consumption is shown on the right side of Fig. 11. Notably, the ADC consumes about 2.0% of the AIMC energy. This efficiency is achieved by sharing ADCs across multiple read-out channels through multiplexing (Xpikeformer uses a sharing ratio of 8, balancing energy efficiency and latency), which significantly reduces the static power consumption that would otherwise be incurred by using dedicated ADCs for each channel. We also observe that the periphery circuits—decoders, multiplexers, switch matrices, buffers, etc., consume 86.0% of the AIMC energy. This is because ADC multiplexing requires a dedicated decoder and control logic, making these components relatively more energy-intensive than the crossbar itself. Additionally, the SA mapping strategy necessitates dedicated mapping control between the shared SRAM and local SA buffers. This overhead is unavoidable in this work due to the crossbar size limitations

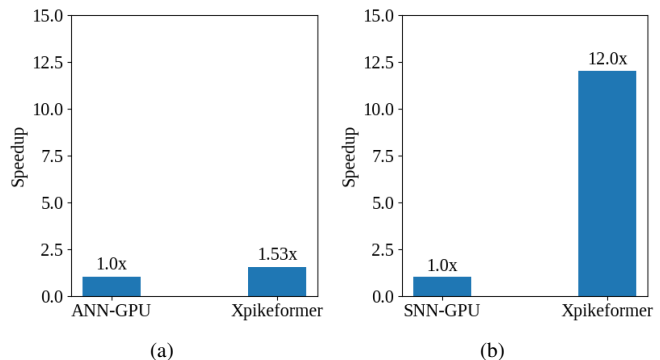


Fig. 12. Speedup of Xpikeformer compared with (a) an ANN Transformer and (b) a spiking transformer deployed on GPU devices.

discussed in Section IV-A. Finally, the accumulation processes, including differential adders and LIF units, which are digital operations, contribute 12.0% of the AIMC energy.

In the two tasks tested, Xpikeformer achieves a 17.8–19.2 \times energy reduction compared to the SOTA digital ANN transformer accelerator (ANN-Digital), a 5.0–7.1 \times energy reduction compared to the hybrid implementation of ANN (ANN-Hybrid), and a 5.9–6.8 \times energy reduction compared to the fully digital implementation of spiking transformers on general-purpose devices (SNN-Digital (no SSA)).

B. Latency Evaluation

We compare the latency of Xpikeformer with two same-sized baseline implementations: an ANN transformer and a spiking transformer deployed on a GPU (Nvidia RTX A2000). We evaluate the runtime per image in Task 1. We adopt a spike encoding length $T = 10$ for both Xpikeformer and the spiking transformer baseline.

Our observations show that Xpikeformer achieves a 1.53 \times speedup compared to the ANN GPU implementation, primarily due to the fast MVM conducted in-memory and the highly parallel and streamlined design of the SSA. Additionally, the spiking transformer exhibits poor time efficiency when deployed on GPU devices due to intrinsic precision mismatches and the lack of dedicated optimization. In contrast, Xpikeformer demonstrates a 12.0 \times speedup over the spiking transformer.

C. FPGA Implementation of SSA

We also implemented the proposed SSA tile on a lightweight FPGA (within Xilinx Zynq-7000 SoC). The latency and power consumption of the FPGA implementation were compared against CPU (Intel i7-12850HX) and GPU (Nvidia RTX A2000), as shown in Table IV. We obtain 48 \times better latency expending 15 \times lesser power than that of the GPU implementation. We also note that the SSA block on FPGA has 18 \times less latency while consuming 17 \times less power than the ANN GPU implementation.

VIII. CONCLUSION

In this paper, we introduced Xpikeformer, a novel hybrid analog-digital hardware architecture designed to accelerate

TABLE IV

COMPARISON OF HARDWARE EFFICIENCY FOR A SINGLE ATTENTION HEAD (CPU AND GPU IMPLEMENTATIONS) FOR DIFFERENT ARCHITECTURES. FOR SSA BLOCK, $T = 10$.

Architecture – Device	f_{clk} (MHz)	Latency (ms)	Power (W)
ANN attention – CPU	2100	0.15	107.01
ANN attention – GPU	562	0.06	26.13
SSA – CPU	2100	2.672	65.54
SSA – GPU	562	0.159	22.41
SSA – FPGA	200	3.3×10^{-3}	1.47

spiking neural network (SNN)-based transformer models. The architecture integrates AIMC for feedforward and fully connected layers and employs a stochastic spiking attention (SSA) engine to efficiently handle the attention mechanism. Our design mitigates the data communication overhead and computational inefficiencies typically associated with deploying spiking transformers on general-purpose platforms.

Xpikeformer demonstrates software-comparable inference accuracy, achieving 84.74% on the CIFAR-10 image classification task and maintaining accuracy above 81% in one year. It also demonstrates software-comparable performance in wireless communication symbol detection tasks. In the two tasks tested, Xpikeformer achieved $17.8\text{--}19.2\times$ energy reduction compared to the state-of-the-art digital ANN transformer accelerator, a $5.0\text{--}7.1\times$ energy reduction compared to the hybrid implementation of ANN, and a $5.9\text{--}6.8\times$ energy reduction compared to the fully digital implementation of spiking transformers on general-purpose devices. Xpikeformer also achieves a $1.53\times$ speedup than traditional ANN on GPU and a $12.0\times$ speedup compared to the GPU implementation of spiking transformers.

In this work, we adopted Neurosim’s crossbar assumption to facilitate energy and latency evaluation. Nevertheless, this approach may not yield the best performance in terms of energy efficiency. Practical implementation of memristor crossbars usually adopts a different input strategy by using the input spikes to drive the conductivity of devices through word lines and using inverted voltage spikes and differential-input ADCs to represent positive and negative values in the crossbar [54].

Future work may include exploring more energy-efficient crossbar designs that better align with state-of-the-art implementations. This could involve investigating alternative input strategies and circuit designs that optimize the use of inverted voltage spikes and differential-input ADCs. Additionally, the integration of advanced memristor technologies and the development of new materials for memristors, e.g., 2-D material, could further enhance the energy efficiency and performance of neuromorphic computing systems [55], [56]. Evaluating the impact of these practical crossbar implementations on the overall system performance and conducting comprehensive real-world testing will be crucial steps in advancing the applicability of Xpikeformer and similar models in energy-constrained environments.

REFERENCES

- [1] A. Vaswani, N. Shazeer, N. Parmar, J. Uszkoreit, L. Jones, A. N. Gomez, L. Kaiser, and I. Polosukhin, “Attention is all you need,” *Advances in neural information processing systems*, vol. 30, 2017.
- [2] A. Dosovitskiy, L. Beyer, A. Kolesnikov, D. Weissenborn, X. Zhai, T. Unterthiner, M. Dehghani, M. Minderer, G. Heigold, S. Gelly, J. Uszkoreit, and N. Houlsby, “An image is worth 16x16 words: Transformers for image recognition at scale,” in *9th International Conference on Learning Representations, ICLR 2021, Virtual Event, Austria, May 3-7, 2021*, 2021.
- [3] M. Zecchin, K. Yu, and O. Simeone, “In-context learning for MIMO equalization using transformer-based sequence models,” in *Proceedings of the Workshop on the Impact of Large Language Models on 6G Networks, IEEE International Conference on Communications (ICC), 2024*.
- [4] V. Rajagopalan, V. T. Kunde, C. S. K. Valmееkam, K. Narayanan, S. Shakkottai, D. Kalathil, and J.-F. Chamberland, “Transformers are efficient in-context estimators for wireless communication,” *arXiv preprint arXiv:2311.00226*, 2023.
- [5] Y. Wang, Z. Gao, D. Zheng, S. Chen, D. Gündüz, and H. V. Poor, “Transformer-empowered 6G intelligent networks: From massive MIMO processing to semantic communication,” *IEEE Wireless Communications*, vol. 30, no. 6, pp. 127–135, 2023.
- [6] C. She and L. Qing, “SpikeFormer: Image reconstruction from the sequence of spike camera based on transformer,” in *ICIGP 2022: The 5th International Conference on Image and Graphics Processing, Beijing, China, January 7 - 9, 2022*. ACM, 2022, pp. 72–78.
- [7] W. Maass, “Networks of spiking neurons: The third generation of neural network models,” *Neural networks*, vol. 10, no. 9, pp. 1659–1671, 1997.
- [8] M. Yao, J. Hu, Z. Zhou, L. Yuan, Y. Tian, B. Xu, and G. Li, “Spike-driven transformer,” in *Advances in Neural Information Processing Systems 36: Annual Conference on Neural Information Processing Systems 2023, NeurIPS 2023, New Orleans, LA, USA, December 10 - 16, 2023*.
- [9] Z. Xu, C. Nie, Z. Deng, Q. Guo, X. Wang, Z. He *et al.*, “SpikeZIP-TF: Conversion is all you need for transformer-based snn,” in *Forty-first International Conference on Machine Learning*, 2024.
- [10] Z. Zhou, Y. Zhu, C. He, Y. Wang, S. Yan, Y. Tian, and L. Yuan, “Spikformer: When spiking neural network meets transformer,” in *The Eleventh International Conference on Learning Representations, ICLR 2023, Kigali, Rwanda, May 1-5, 2023*.
- [11] C. Zhou, L. Yu, Z. Zhou, Z. Ma, H. Zhang, H. Zhou, and Y. Tian, “Spikingformer: Spike-driven residual learning for transformer-based spiking neural network,” *arXiv preprint arXiv:2304.11954*, 2023.
- [12] Z. Zhou, K. Che, W. Fang, K. Tian, Y. Zhu, S. Yan, Y. Tian, and L. Yuan, “Spikformer V2: join the high accuracy club on imagenet with an SNN ticket,” *arXiv preprint arXiv:2401.02020*, 2024.
- [13] M. Bal and A. Sengupta, “Spikingbert: Distilling bert to train spiking language models using implicit differentiation,” in *Proceedings of the AAAI conference on artificial intelligence*, vol. 38, no. 10, 2024, pp. 10 998–11 006.
- [14] R.-J. Zhu, Q. Zhao, G. Li, and J. K. Eshraghian, “SpikeGPT: Generative pre-trained language model with spiking neural networks,” *arXiv preprint arXiv:2302.13939*, 2023.
- [15] J. Zhang, B. Dong, H. Zhang, J. Ding, F. Heide, B. Yin, and X. Yang, “Spiking Transformers for Event-Based Single Object Tracking,” in *Proceedings of the IEEE/CVF Conference on Computer Vision and Pattern Recognition*, 2022, pp. 8801–8810.
- [16] M. Yao, J. Hu, Z. Zhou, L. Yuan, Y. Tian, B. Xu, and G. Li, “Spike-driven transformer,” *Advances in Neural Information Processing Systems*, vol. 36, 2024.
- [17] Z. Song, P. Katti, O. Simeone, and B. Rajendran, “Stochastic spiking attention: Accelerating attention with stochastic computing in spiking networks,” in *2024 IEEE 6th international conference on artificial intelligence circuits and systems (AICAS)*, 2024.
- [18] A. Sebastian, M. Le Gallo, R. Khaddam-Aljameh, and E. Eleftheriou, “Memory devices and applications for in-memory computing,” *Nature nanotechnology*, vol. 15, no. 7, pp. 529–544, 2020.
- [19] X. Yang, B. Yan, H. Li, and Y. Chen, “ReTransformer: ReRAM-based Processing-in-Memory Architecture for Transformer Acceleration,” in *2020 IEEE/ACM International Conference On Computer Aided Design (ICCAD)*, 2020, pp. 1–9.
- [20] C. Yang, X. Wang, and Z. Zeng, “Full-circuit implementation of transformer network based on memristor,” *IEEE Transactions on Circuits and Systems I: Regular Papers*, vol. 69, no. 4, pp. 1395–1407, 2022.
- [21] S. Sridharan, J. R. Stevens, K. Roy, and A. Raghunathan, “X-former: In-memory acceleration of transformers,” *IEEE Transactions on Very Large Scale Integration (VLSI) Systems*, vol. 31, no. 8, pp. 1223–1233, 2023.
- [22] E. J. Merced-Grafals, N. Dávila, N. Ge, R. S. Williams, and J. P. Strachan, “Repeatable, accurate, and high speed multi-level program-

- ming of memristor 1T1R arrays for power efficient analog computing applications,” *Nanotechnology*, vol. 27, no. 36, p. 365202, 2016.
- [23] B. R. Gaines, “Techniques of identification with the stochastic computer,” in *Proc. International Federation of Automatic Control Symposium on Identification, Progue*, 1967.
- [24] A. Alaghi and J. P. Hayes, “Survey of stochastic computing,” *ACM Transactions on Embedded Computing Systems*, vol. 12, no. 2s, pp. 1–19, 2013.
- [25] J. Devlin, M.-W. Chang, K. Lee, and K. Toutanova, “BERT: Pre-training of deep bidirectional transformers for language understanding,” in *Proceedings of the 2019 Conference of the North American Chapter of the Association for Computational Linguistics: Human Language Technologies, Volume 1*, 2019, pp. 4171–4186.
- [26] T. Brown, B. Mann, N. Ryder, M. Subbiah, J. D. Kaplan, P. Dhariwal, A. Neelakantan, P. Shyam, G. Sastry, A. Askell *et al.*, “Language models are few-shot learners,” *Advances in neural information processing systems*, vol. 33, pp. 1877–1901, 2020.
- [27] Z. Song, O. Simeone, and B. Rajendran, “Neuromorphic in-context learning for energy-efficient MIMO symbol detection,” *arXiv preprint arXiv:2404.06469*, 2024.
- [28] M. Isik, H. Vishwamith, K. Inadagbo, and I. Dikmen, “HPCNeuroNet: Advancing neuromorphic audio signal processing with transformer-enhanced spiking neural networks,” *arXiv preprint arXiv:2311.12449*, 2023.
- [29] X. Peng, S. Huang, H. Jiang, A. Lu, and S. Yu, “DNN+NeuroSim V2.0: An end-to-end benchmarking framework for compute-in-memory accelerators for on-chip training,” *IEEE Transactions on Computer-Aided Design of Integrated Circuits and Systems*, vol. 40, no. 11, pp. 2306–2319, 2020.
- [30] H. Shao, J. Lu, M. Wang, and Z. Wang, “An efficient training accelerator for transformers with hardware-algorithm co-optimization,” *IEEE Transactions on Very Large Scale Integration (VLSI) Systems*, vol. 31, no. 11, pp. 1788–1801, 2023.
- [31] A. Marchisio, D. Dura, M. Capra, M. Martina, G. Masera, and M. Shafique, “SwiftTron: An efficient hardware accelerator for quantized transformers,” in *2023 International Joint Conference on Neural Networks (IJCNN)*, 2023, pp. 1–9.
- [32] T. J. Ham, S. J. Jung, S. Kim, Y. H. Oh, Y. Park, Y. Song, J.-H. Park, S. Lee, K. Park, J. W. Lee, and D.-K. Jeong, “A³: Accelerating attention mechanisms in neural networks with approximation,” in *2020 IEEE International Symposium on High Performance Computer Architecture (HPCA)*, 2020, pp. 328–341.
- [33] H.-Y. Wang and T.-S. Chang, “Row-wise accelerator for vision transformer,” in *2022 IEEE 4th International Conference on Artificial Intelligence Circuits and Systems (AICAS)*, 2022, pp. 399–402.
- [34] J. Park, H. Yoon, D. Ahn, J. Choi, and J.-J. Kim, “OPTIMUS: OPTimized matrix MUltiplication Structure for Transformer neural network accelerator,” *Proceedings of Machine Learning and Systems*, vol. 2, pp. 363–378, 2020.
- [35] A. Okazaki, P. Narayanan, S. Ambrogio, K. Hosokawa, H. Tsai, A. Nomura, T. Yasuda, C. Mackin, A. Friz, M. Ishii *et al.*, “Analog-memory-based 14nm hardware accelerator for dense deep neural networks including transformers,” in *2022 IEEE International Symposium on Circuits and Systems (ISCAS)*, 2022, pp. 3319–3323.
- [36] K. Spoon, H. Tsai, A. Chen, M. J. Rasch, S. Ambrogio, C. Mackin, A. Fasoli, A. M. Friz, P. Narayanan, M. Stanisavljevic *et al.*, “Toward software-equivalent accuracy on transformer-based deep neural networks with analog memory devices,” *Frontiers in Computational Neuroscience*, vol. 15, p. 675741, 2021.
- [37] M. Zhou, W. Xu, J. Kang, and T. Rosing, “TransPIM: A memory-based acceleration via software-hardware co-design for transformer,” in *2022 IEEE International Symposium on High-Performance Computer Architecture (HPCA)*, 2022, pp. 1071–1085.
- [38] W. Li, M. Manley, J. Read, A. Kaul, M. S. Bakir, and S. Yu, “H3DAtten: Heterogeneous 3-D integrated hybrid analog and digital compute-in-memory accelerator for vision transformer self-attention,” *IEEE Transactions on Very Large Scale Integration (VLSI) Systems*, 2023.
- [39] M. Bouvier, A. Valentian, T. Mesquida, F. Rummens, M. Reyboz, E. Vianello, and E. Beigne, “Spiking neural networks hardware implementations and challenges: A survey,” *ACM Journal on Emerging Technologies in Computing Systems (JETC)*, vol. 15, no. 2, pp. 1–35, 2019.
- [40] A. Carpegna, A. Savino, and S. Di Carlo, “Spiker: an FPGA-optimized hardware accelerator for spiking neural networks,” in *2022 IEEE Computer Society Annual Symposium on VLSI (ISVLSI)*, 2022, pp. 14–19.
- [41] Y. Liu, Y. Chen, W. Ye, and Y. Gui, “FPGA-NHAP: A general fpga-based neuromorphic hardware acceleration platform with high speed and low power,” *IEEE Transactions on Circuits and Systems I: Regular Papers*, vol. 69, no. 6, pp. 2553–2566, 2022.
- [42] J. Wu, Y. Chen, W. S. Khwa, S. M. Yu, T. Y. Wang, J. Tseng, Y. Chih, and C. H. Diaz, “A 40nm low-power logic compatible phase change memory technology,” in *2018 IEEE International Electron Devices Meeting (IEDM)*, 2018, pp. 27.6.1–27.6.4.
- [43] H.-S. P. Wong, S. Raoux, S. Kim, J. Liang, J. P. Reifenberg, B. Rajendran, M. Asheghi, and K. E. Goodson, “Phase change memory,” *Proceedings of the IEEE*, vol. 98, no. 12, pp. 2201–2227, 2010.
- [44] A. Mehonic, A. Sebastian, B. Rajendran, O. Simeone, E. Vasilaki, and A. J. Kenyon, “Memristors—from in-memory computing, deep learning acceleration, and spiking neural networks to the future of neuromorphic and bio-inspired computing,” *Advanced Intelligent Systems*, vol. 2, no. 11, p. 2000085, 2020.
- [45] P. Katti, A. Nimbekar, C. Li, A. Acharyya, B. M. Al-Hashimi, and B. Rajendran, “Bayesian inference accelerator for spiking neural networks,” in *IEEE International Symposium on Circuits and Systems, ISCAS 2024, Singapore, May 19-22, 2024*, pp. 1–5.
- [46] Pseudo Random Number Generation Using Linear Feedback Shift Registers. Accessed on 20/10/2023. [Online]. Available: <https://www.analog.com/en/design-notes/random-number-generation-using-lfsr.html>
- [47] W. Fang, Y. Chen, J. Ding, Z. Yu, T. Masquelier, D. Chen, L. Huang, H. Zhou, G. Li, and Y. Tian, “Spikingjelly: An open-source machine learning infrastructure platform for spike-based intelligence,” *Science Advances*, vol. 9, no. 40, p. eadi1480, 2023.
- [48] M. J. Rasch, D. Moreda, T. Gokmen, M. Le Gallo, F. Carta, C. Goldberg, K. El Maghraoui, A. Sebastian, and V. Narayanan, “A flexible and fast pytorch toolkit for simulating training and inference on analog crossbar arrays,” in *2021 IEEE 3rd international conference on artificial intelligence circuits and systems (AICAS)*, 2021, pp. 1–4.
- [49] D. P. Kingma and J. Ba, “Adam: A method for stochastic optimization,” in *3rd International Conference on Learning Representations, ICLR 2015, San Diego, CA, USA, May 7-9, 2015, Conference Track Proceedings*, 2015.
- [50] V. Joshi, M. Le Gallo, S. Haefeli, I. Boybat, S. R. Nandakumar, C. Piveteau, M. Dazzi, B. Rajendran, A. Sebastian, and E. Eleftheriou, “Accurate deep neural network inference using computational phase-change memory,” *Nature communications*, vol. 11, no. 1, p. 2473, 2020.
- [51] A. Pedram, S. Richardson, M. Horowitz, S. Galal, and S. Kvatinsky, “Dark memory and accelerator-rich system optimization in the dark silicon era,” *IEEE Design & Test*, vol. 34, no. 2, pp. 39–50, 2017.
- [52] C. Buffa, L. Hernandez-Corporales, C. A. P. Cruz, A. Q. Alonso, and A. Wiesbauer, “Voltage controlled oscillator based analog-to-digital converter including a maximum length sequence generator,” Jan. 5 2021, US Patent 10,886,930.
- [53] G. Datta, S. Kundu, A. R. Jaiswal, and P. A. Beerel, “ACE-SNN: Algorithm-hardware co-design of energy-efficient & low-latency deep spiking neural networks for 3d image recognition,” *Frontiers in Neuroscience*, vol. 16, 2022.
- [54] Y.-C. Chiu, H.-W. Hu, L.-Y. Lai, T.-Y. Huang, H.-Y. Kao, K.-T. Chang, M.-S. Ho, C.-C. Chou, Y.-D. Chih, T.-Y. Chang, and M.-F. Chang, “A 40nm 2Mb ReRAM macro with 85% reduction in FORMING time and 99% reduction in page-write time using auto-FORMING and auto-write schemes,” in *2019 Symposium on VLSI Technology*, 2019, pp. T232–T233.
- [55] S. Chen, M. R. Mahmoodi, Y. Shi, C. Mahata, B. Yuan, X. Liang, C. Wen, F. Hui, D. Akinwande, D. B. Strukov *et al.*, “Wafer-scale integration of two-dimensional materials in high-density memristive crossbar arrays for artificial neural networks,” *Nature Electronics*, vol. 3, no. 10, pp. 638–645, 2020.
- [56] Z. Dong, Q. Hua, J. Xi, Y. Shi, T. Huang, X. Dai, J. Niu, B. Wang, Z. L. Wang, and W. Hu, “Ultrafast and low-power 2d bi2o2se memristors for neuromorphic computing applications,” *Nano Letters*, vol. 23, no. 9, pp. 3842–3850, 2023.